Int. J. Heat Mass Transfer. Vol. 28, No. 7, pp. 1281–1292, 1985
Printed in Great Britain

0017-9310/85 $3.00 + 0.00

Inverted annular boiling in a stainless-steel tube with steady heat sources

Z. EDELMAN, E. ELIAS and D. NAOT*
Department of Nuclear Engineering, Technion, Haifa, 32000, Israel

(*Received* 15 *June* 1984 *and in final form* 10 *December* 1984)

Abstract—Simultaneous measurements of wall temperatures and vapor film thicknesses in an inverted annular film boiling are reported. The data correspond to bottom reflooding of a single tube uniformly heated with a steady electric heat source. The raw data are processed to yield the wall heat flux, heat transfer coefficient, quench front velocity, quench front temperature and void fraction, which may serve as a relatively complete comparative base for the development of theoretical models.

INTRODUCTION

DURING a postulated loss of coolant accident (LOCA) in light water reactors (LWRs), the fuel cladding may experience a rapid increase in temperature as a result of a change in heat transfer mode from nucleate boiling to the less effective film boiling. The subsequent injection of emergency core coolant brings about a series of heat and mass transfer processes which eventually reflood the channel after cooling the hot surface below the quenching or rewetting temperature. Two types of flow patterns may exist during reflooding, depending on the inlet flow rate, inlet subcooling and the rate of heat generation in the fuel pins. The flow pattern shown in Fig. 1 is called the inverted annular film boiling regime. It is characterized by a continuous liquid core separated from the wall by a vapor film above the quench front. Enhanced heat transfer in the vapor film is believed to result from film and liquid core instabilities and droplet entrainment. The velocity within the vapor film increases downstream of the quench front until, at some point, it reaches a critical value which causes the liquid core to break into liquid droplets and globules [1, 2]. A second flow pattern may occur during reflood in which a dispersed flow film boiling region exists just above the quench front.

The reflooding phase of the LOCA has been the subject of an extensive amount of studies in the last decade [3–5]. The need for an accurate mechanistic modeling of this phase has prompted several laboratory-scale experiments to study the details of the mass and heat transfer processes taking place in the vicinity of the quench front [6–8]. Mechanistic modeling of the heat transfer coefficient in the inverted annular film boiling regime has been shown to rely on detailed information on the phases velocity and the flow and temperature distributions in the liquid core and the vapor film regions [8, 9]. Preliminary experimental data on these parameters have been presented by the authors [10]. The present work is concentrated mainly on the experimental investigation of the inverted annular region. An experimental reflooding program was undertaken on a single tube with constant inlet conditions and heat generation [11]. Two types of measurements were carried out locally above the quench front: temperature–time trajectories along the tube outer surface and void fraction or vapor film thickness history.

The measurements enabled better understanding of the complex heat transfer phenomena taking place in the inverted annular region as the data could be processed to yield simultaneously the wall heat flux, the heat transfer coefficient, the quench front velocity, and the quench front temperature. The data is reported in the form of graphs and semiempirical correlations which cover the experimental range. A theoretical derivation based on the measured data and on a two-fluid model was used in order to verify the consistency of the two different experimental systems used to

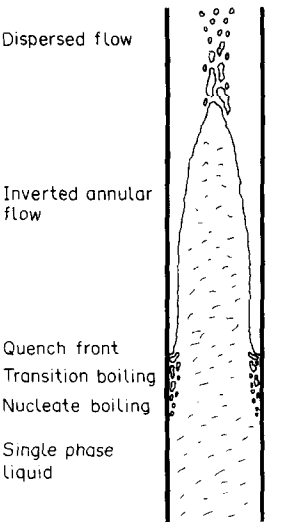

FIG. 1. Schematic illustration of an inverted annular film boiling regime.

*Current address: The Center for Technological Education, P.O. Box 305, Holon, 58102, Israel.

NOMENCLATURE

a	dimensionless constant
c_p	specific heat at constant pressure
D	pipe diameter
D_i	pipe inner diameter
G	coolant inlet mass flux
h	heat transfer coefficient; flow enthalpy
h_0	reference heat transfer coefficient
I	gamma beam intensity
k	thermal conductivity
$\dot{m}$	mass flow rate
P	probability of liquid penetration
p	pressure
q'	linear heat generation rate
q''	surface heat flux
q'''	volumetric heat generation rate
q''_p	heat absorption potential
R	pipe radius
T	temperature
T_q	quench front temperature
t	time
X	flow quality
Z	axial coordinate.

Greek symbols

α	void fraction
δ	film thickness
ε	emissivity
ζ	dimensionless distance along flow path
θ	dimensionless temperature
ρ	density
τ	characteristic time; shear stress.

Subscripts

a	environment
e	electric
g	vapor phase
i	interface
in	inlet property
l	liquid phase
max	maximum value
min	minimum value
o	outer surface
qf	quench front
rad	radiation
ref	reference
s	saturation
w	wall.

Superscript

0	initial value.

measure the temperature trajectories and the void fraction. Although the confidence in identifying the inverted annular regime is substantially increased due to the simultaneous measurements, the interpretation of the data is still restricted to perfect annular geometry ignoring the possibility that the liquid core may assume a helical configuration.

EXPERIMENTAL APPARATUS AND PROCEDURES

The experimental set-up consisted of a vertical stainless-steel (304) tube 2 m (6 ft) long with an outside diameter of 12.7 mm. Measurements were taken in two different tubes with wall thicknesses of 0.7 and 0.9 mm, respectively. The general layout of the major components is shown schematically in Fig. 2. A bare tube was used heated electrically through flanges at both ends by a 10 kWA stabilized DC power supply. The power input was measured by monitoring the voltage across the test section and the current across a shunt in series to the tube. A close-coupled turbine-pump was used to provide a steady forced flow of subcooled distilled water to the bottom of the test section. The flow rate was regulated by a set of bypasses and throttling valves. The water was heated in a storage tank to a predetermined temperature before each experiment.

The measurement system included temperature measurements by chromel–alumel (Type K AWG-30) thermocouples spot welded 1.5 cm (0.05 ft) apart on the outside of the test section. Absolute pressure at the bottom of the tube was measured by a fast response strain gauge (Validyne CD 15-C). Data acquisition was performed with a PDP 11/34 computer connected to a hard disk. Special computer programs were used to convert the raw data into engineering units and to use the reduced data in heat flux and flow rate calculations.

The volumetric void fraction distribution downstream of the quench front was measured by a

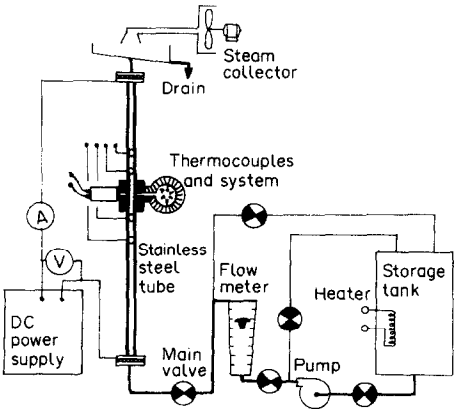

FIG. 2. Experimental set-up and test apparatus.

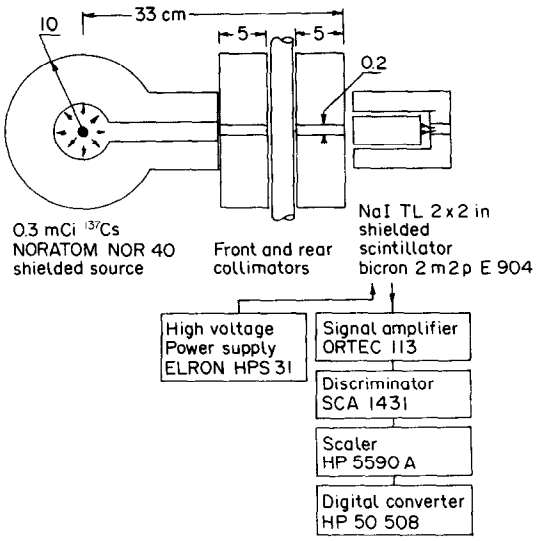

FIG. 3. The gamma densitometer and the electronic counting system.

stationary gamma densitometer. This technique is based on measuring the intensity of a narrow gamma beam transmitted through the flow channel. The densitometer consisted of a collimated 330 mCi ^{137}Cs gamma source. The source and detector collimators defined a narrow beam, 2 mm in diameter, traversing along the tube diameter. The system configuration is schematically illustrated in Fig. 3 which also indicates the major components of the detection electronics.

In an axisymetric inverted annular flow configuration the void fraction can be readily determined from the densitometer response by:

$$\alpha = 1 - \left[\frac{\ln(I_{max}/I)}{\ln(I_{max}/I_{min})}\right] \quad (1)$$

where I_{max} and I_{min} are reference beam intensities for $\alpha = 0$ and $\alpha = 1$, respectively. The reference intensities were measured before and after each experiment to minimize errors due to electronic drifts.

The measurement error in α is determined predominantly by the statistical counting errors. In the present system the count rate was about 32,000 counts s^{-1}. For 1 s measuring time the relative error in α due to counting statistics was 7%. Considering other sources of errors, such as deviation from axisymmetric flow, the total relative error in α is estimated to be about 10%. The measured intensities, I were smoothed, by fitting the data sectionally to a continuous and monotonous function, before substituting in equation (1) to calculate α.

The average thickness δ of the vapor film downstream of the quench front is determined from α by:

$$\delta = \frac{D}{2}[1 - \sqrt{1-\alpha}]. \quad (2)$$

The error in δ is related to the error in α by:

$$\Delta(\delta) = \frac{D}{4}\frac{\Delta(\alpha)}{\sqrt{1-\alpha}} \quad (3)$$

where Δ signifies an absolute error.

The main initial conditions for a selected set of 23 different experiments performed with the two tubes are listed in Table 1. The test plan was chosen to embrace parametric values expected in accident conditions. Measurements were carried out at atmospheric pressure, inlet mass flux in the range 80–250 kg m^{-2} s^{-1}, initial wall temperature of up to 750°C and inlet liquid temperature 15–22°C (subcooling of 85–78°C, respectively). As the wall thickness and the emissivity of the two tubes used in the experiment were different two different sets of electrical power, also given in Table 1, were applied to establish the initial wall temperatures specified in the table.

WALL TEMPERATURE TRAJECTORIES

The thermal and hydraulic response of the tube undergoing reflooding is discussed in this chapter in terms of its initial and inlet conditions. Wall temperature histories at a fixed location about 1 m from the tube inlet are shown in Fig. 4 for the two wall thicknesses and varying inlet mass flux as a function of time difference from quenching. Results are plotted for initial wall temperature of 650 to 675°C and inlet water

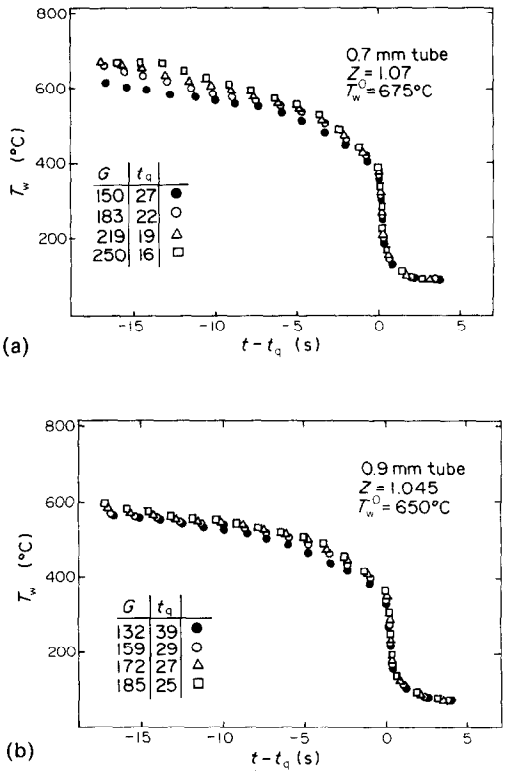

FIG. 4. Typical wall temperature trajectories for (a) 0.7-mm tube and (b) 0.9-mm tube with different inlet mass flux.

Table 1. Experimental data and set-up of the experiments

Wall thickness (mm)	Inlet subcooling (°C)	Initial wall temperature (°C)	Linear power (kW m^{-1})	Inlet mass flux (kg m^{-2} s^{-1})	Test No.
				124	1
		590	1.936	161	2
				196	3
				132	4
				159	5
0.9	83	650	2.35	172	6
				185	7
(O.D. = 12.7)					
				161	8
				196	9
		750	3.2	234	10
				268	11
				83	12
		560	1.31	115	13
				150	14
				183	15
				150	16
0.7	78	675	1.96	183	17
				219	18
(O.D. = 12.7)				250	19
				150	20
				183	21
		770	2.92	219	22
				250	23

temperature of 17 to 22°C. The wall temperature stays relatively constant until approx. 15 s before quenching. Later, a gradual decrease of temperature is observed due to precursory cooling by steam produced at the lower part of the tube. At a given elevation, the gradual decrease in the wall temperature continues until the tube quenches, at which time the wall temperature drops sharply to a steady value which corresponds to the fluid temperature at that elevation.

The time for the quench front to reach a specific location on the tube (quenching time) depends strongly on the inlet mass flux as indicated in the legend to Fig. 4. For a given initial wall temperature and inlet subcooling, the quenching time is inversely proportional to the inlet mass flux. The wall thickness has a second-order effect in the studied range of parameters. The thicker pipe (0.9-mm wall) takes slightly longer time to quench due to its higher stored energy.

Figure 5 shows the effect of the initial wall temperature on the wall temperature histories for given inlet water flux and subcooling. Reducing the initial wall temperature reduces the time it takes for a specific location on the tube to undergo quenching. Qualitatively similar results were obtained for the thicker (0.9-mm) wall tube. It is of interest to note that the influence of the wall initial temperature on the wall temperature profile diminishes towards the quenching zone. More detailed description of this effect is given later.

Finally, three temperature trajectories for the same experiment taken at three different elevations from the tube inlet are given in Fig. 6, for an initial wall temperature of 675°C and inlet mass flux of 183 kg m^{-2} s^{-1}. The remarkable similarity between the three temperature–time histories supports the assumption that it is possible to estimate spatial temperature distributions from the time trajectories. The quenching times, also given in Fig. 6, suggest that in the test section elevation between 0.9 to 1.27 m we may expect that the variations in the quench front velocity are less than 10%.

The measured temperature–time trajectories were utilized to calculate the quench front propagation velocity. The propagation times between two

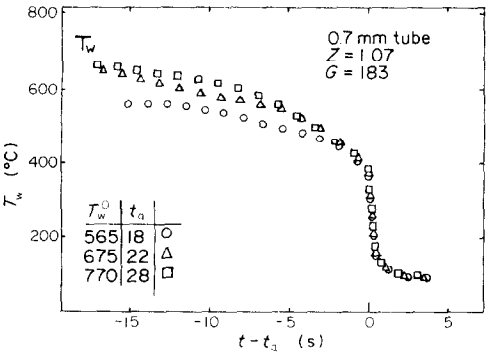

FIG. 5. Wall temperature trajectories for different initial wall temperatures.

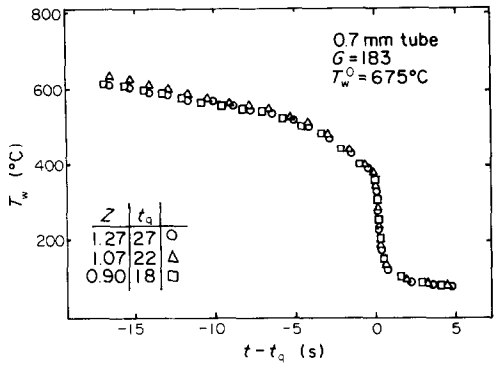

FIG. 6. Wall temperature trajectories measured at different elevations.

thermocouples located 15 cm apart were determined for each run and used to calculate the local quench front velocity. Figures 7(a) and (b) present the normalized quench front velocity as a function of the initial wall temperature for the two wall thicknesses studied. The ratio of the quench front velocity and inlet liquid velocity V_{qf}/V_{in} is shown to depend mainly on the initial wall temperature, T_w^0. The effect of the inlet mass flux is shown to be of second order. It should be noted, however, that the test matrix studied does not cover a wide enough range of inlet subcooling to allow for a systematic study of the effect of this parameter. The normalized quench front velocity data in Figs. 7(a) and 7(b) can be summarized by the following correlations:

$$\frac{V_{qf}}{V_{in}} = \begin{cases} 0.62(1-0.11\theta_w) & \text{for the 0.7-mm tube} \\ 0.6(1-0.12\theta_w) & \text{for the 0.9-mm tube} \end{cases} \quad (4)$$

with

$$\theta_w = \frac{T_w^0 - T_s}{T_s}. \quad (5)$$

Equation (4) is applicable for the present experiment only in the range $3 < \theta_w < 7$. It implies that for high initial wall temperature the quench front velocity vanishes and a static quench front may be established. However, the extrapolation of the data towards a static quench front should be made with care as we expect that with the reduction of the quench front velocity the precursory cooling of the wall by the dispersed flow regime would have enough time to alter the wall temperature downstream of the quench front from its initial value to a new equilibrium state.

The wall temperature just downstream of the quench front is of importance for theoretical modeling of the rewetting problem. This temperature is sometimes called rewetting or quenching temperature and is identified with either the critical heat flux or the minimum film boiling temperature [4, 5]. Quench temperatures were established in this study by the intersection of tangent lines that define the slopes of the temperature–time trajectories before and after the quench zone. Figures 8(a) and 8(b) show the quenching temperature vs the initial wall temperature. All measurements are reported at around the 1-m elevation. It is demonstrated that for both tubes the quenching temperature is mainly a function of the initial wall temperature with minor effects of the inlet mass flux and wall thickness. Note however, that the present experimental definition of the quench

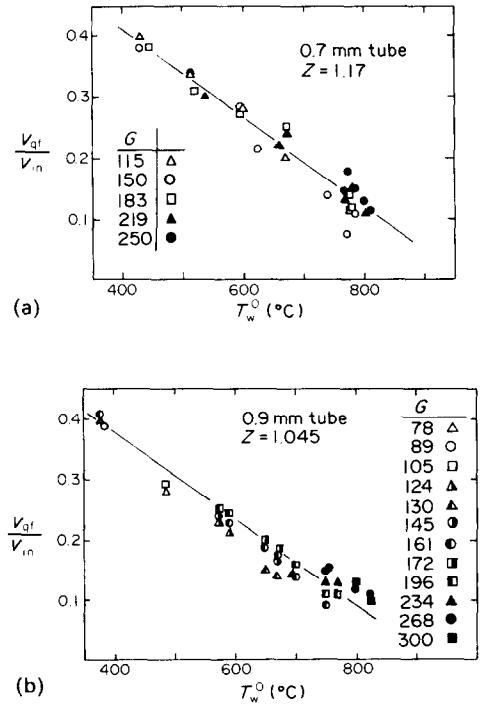

FIG. 7. Quench front velocities for (a) 0.7-mm tube and (b) 0.9-mm tube as a function of the initial wall temperature.

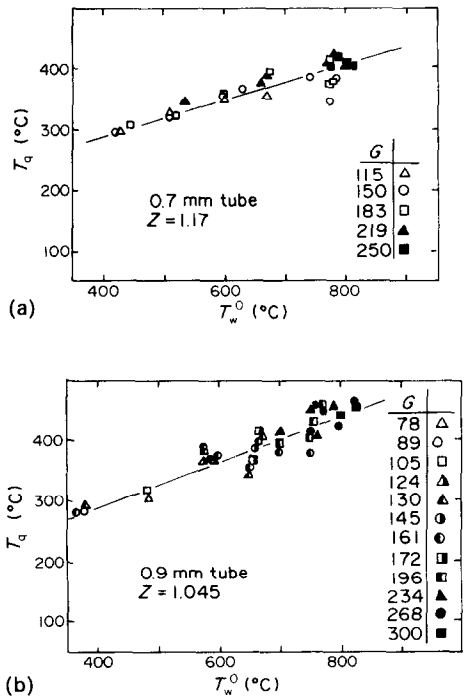

FIG. 8. Quench front temperature for (a) 0.7-mm tube and (b) 0.9-mm tube as a function of the initial wall temperature.

temperature is somewhat arbitrary, mainly in respect to the slope of the temperature–time curve obtained before the rapid quench cooling begins. Accepting this we may suggest the following correlation:

$$\frac{T_q - T_s}{T_s} = \begin{cases} 1.1 + 0.28\theta_w & \text{for the 0.7-mm tube} \\ 0.9 + 0.33\theta_w & \text{for the 0.9-mm tube} \end{cases} \quad (6)$$

which fits the present results in the range $3 < \theta_w < 7$.

Equation (6) implies that the ratio between the quench front temperature and the initial wall temperature decreases with increasing the initial wall temperature. For high initial temperature a limiting value of about 1/3 is reached. It is to be noted however, that although similar behavior of the quenching temperature has been reported by Yu [12], equation (6) is applicable only in the particular geometry and range of conditions of the present experiment. There is often variation of this temperature over the height of the tube during any one run. The use of equation (6) for an initial temperature lower than the specified range is not realistic.

WALL HEAT FLUX

As the wall heat flux cannot be measured directly it was derived from a heat balance. To this end a one-dimensional time-dependent analysis was applied to the thin tube relating the wall heat flux to the vapor film q''_w to the wall temperature–time trajectory T_w:

$$q''_w = \left(\frac{D_o^2 - D_i^2}{4D_i}\right)\left(q'''_e - \rho_w c_{pw}\frac{\partial T_w}{\partial t} + k_w\frac{\partial^2 T_w}{\partial Z^2}\right) - \frac{D_o}{D_i}h_a(T_w - T_a). \quad (7)$$

The tubes' parameters considered are the external and internal diameters D_o and D_i, the wall specific density ρ_w, the wall specific heat capacity c_{pw}, and the wall conductivity k_w. The heat losses to the environment at temperature T_a were calculated using an experimental heat transfer coefficient h_a, considering also the electrical heat sources q''_p.

To evaluate the axial conduction we note the plausibility of the assumption that the quench front velocity and the temperature trajectories do not change during the period of time relevant to the present analysis. We therefore may replace the axial convection term in equation (7) by

$$k_w\frac{\partial^2 T_w}{\partial Z^2} \simeq \frac{k_w}{V_{qf}^2}\frac{\partial^2 T_w}{\partial t^2} \quad (8)$$

and estimate its relative importance by:

$$k_w\frac{\partial^2 T_w}{\partial Z^2}\Big/\rho_w c_{pw}\frac{\partial T_w}{\partial t} = 0\left(\frac{k_w}{\rho_w c_{pw} V_{qf}^2 \tau}\right). \quad (9)$$

With typical time scale τ taken as 1 s the relative magnitude of the axial conduction is determined by equation (9) to be of the order of 0.02 which justifies its neglection.

To evaluate experimentally the loss heat transfer coefficient h_a we note that in the absence of fluid flow, steady state is reached when the heat losses to the laboratory balance the electrical heat sources:

$$h_a(T_w - T_a) = \frac{D_o^2 - D_i^2}{4D_o}q'''_e. \quad (10)$$

With the measured wall temperature and the electrical current and voltage across the test section, the electrical heat source was calculated and the heat transfer coefficient h_a was found using equation (10). The results of a series of experiments were least-square fitted as a function of the wall temperature by:

$$h_a = 0.184T_w - 3.13\times10^{-4}T_w^2 + 3.75\times10^{-7}T_w^3. \quad (11)$$

Here T_w is given in °C and h_a in W m^{-2} °C^{-1}. Equation (11) completes the specification of all the parameters of equation (7) in terms of the wall temperature and the derivation of the wall heat flux becomes possible.

The heat flux shown in Figs. 9(a–c) is given in terms of a local convective heat transfer coefficient h. To obtain this we had to substract from the total heat flux the heat transferred from the wall to the liquid core by direct radiation q''_{rad}, and to specify a reference temperature for the vapor film. In the absence of experimental data for the mixed-cup temperature, which is preferable for such purpose, we selected the saturation temperature which characterizes the vapor at the liquid side of the annular film. Subjected to this choice the heat transfer coefficient is calculated from:

$$h = (q''_w - q''_{rad})/(T_w - T_s). \quad (12)$$

A remarkable feature that shows up in Fig. 9 is the observation that when plotted in terms of the distance from the quench front, the temperature trajectories almost do not depend on the inlet mass flux. On the other hand, the predicted heat transfer coefficients depend on G since it is calculated from the temperature–time trajectories which do depend on G. Note that for the sake of clarity the data points are omitted in Fig. 9. Rather, the calculated trends are illustrated by smooth lines which fit the data. Generally, the scattering of the predicted heat transfer coefficients was less than 10%. The data scattering was mainly a result of the smoothing procedure used to evaluate the time derivative of the temperature in equation (10).

VAPOR FILM THICKNESS

The main advantage in taking simultaneous measurements for both the wall temperature and the void fraction is the ability to differentiate between the annular and inverted annular film boiling regime. In the annular film boiling regime a dramatic reduction in the wall temperature typically precedes the rapid drop of the void fraction. On the other hand, in the inverted annular film boiling regime quenching takes place

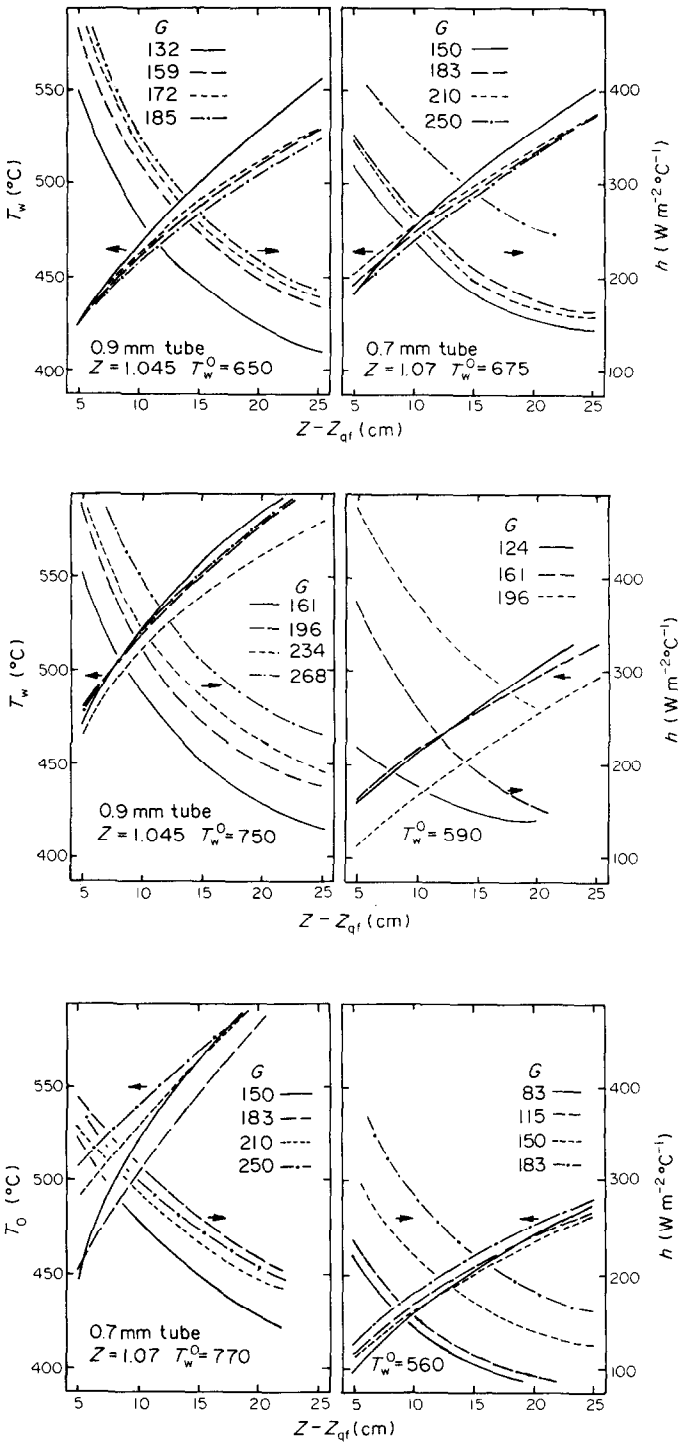

FIG. 9. Wall temperature and heat transfer coefficient as a function of distance from the quench front for the 0.7-mm tube at different initial wall temperatures and inlet mass flux.

in a relatively low void fraction condition. Based on the present set of experiments it seems that the necessary conditions for the existence of an inverted annular film boiling regime are: flooding rate greater than 75 kg m^{-2} s^{-1} and equilibrium quality just below the quench front less than -0.05. The evaluation of the latter is described in Appendix B. The existence of an inverted annular film boiling regime was also verified by comparing the collapsed liquid level, measured by the pressure transducer at the bottom of the test section, with the location of the quench front detected by the wall temperature trajectories.

The measured void fraction and the corresponding vapor film thickness [equation (2)] are given in Fig. 10

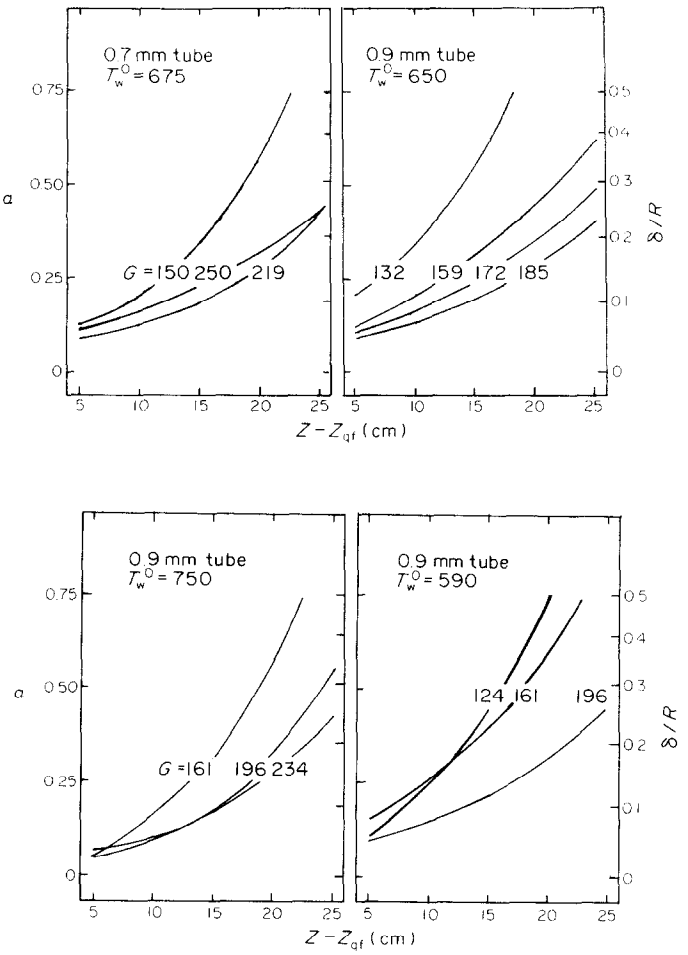

FIG. 10. Void fraction and vapor film thickness as a function of distance from the quench front.

as a function of the distance downstream of the quench front and the inlet water mass flux. Note that either the void fraction or the film thickness can be obtained from any curve in Fig. 10 by appropriate choice of the left or right ordinate axis. Here again the data points are omitted for the sake of clarity. Generally, data scattering of up to 10% (relative) were observed in both the void fraction and film thickness. It is noticed that the slope of the curves in Fig. 10 is not constant. Close to the quench front the vapor film thickness is almost constant and only at distances greater than about 10 cm it starts to develop rapidly. The rate of increase of the vapor film thickness is inversely proportional to the inlet mass flux, with a less pronounced influence of the initial wall temperature. It is to be noted that void fractions of more than 0.5 are probably not in a truly inverted annular flow regime. The discrepancy between some of the curves in Fig. 10 is presumably due to the liquid core eccentricity.

As mentioned before, in the present study both the heat flux and the vapor film thickness were measured simultaneously. This poses an obligation to show the consistency of the experimental data which were achieved by two substantially different means. To this end a two-fluid model was constructed and solved numerically using a forward marching scheme with iteration performed within each step to overcome the nonlinearity of the equations. The model which is similar to that proposed by Chan and Yadigaroglu [13] is described in Appendix A. It considers the experimental heat flux and the experimental initial conditions to yield the axial distribution of the vapor volume fraction. Some results are shown in Fig. 11 describing the ratio between the calculated and measured film thickness as a function of distance from the quench front. Generally, the level of agreement between the model prediction and the experimental data was similar to that shown for test number 6, supporting qualitatively the consistency of the experimental data. Two extreme cases are also shown in Fig. 11. Test 9 is an example in which the initial film thickness is overestimated and in Test 10 the initial film thickness is underestimated. However, since the heat transfer to the liquid core is inversely proportional to the film thickness, the deviations between the predicted and measured film thicknesses diminish downstream of the quench front. Even in the two extreme cases shown in Fig. 11 the predicted film thicknesses at distances,

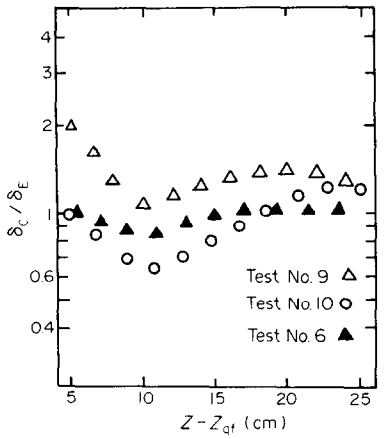

FIG. 11. Comparison between calculated and measured vapor film thickness.

$Z-Z_{qf}$, greater than 10 cm are in fair agreement with the measurements.

HEAT TRANSFER CORRELATION

To enable a simple use of the present experimental information on the inverted annular film boiling heat transfer it is necessary to describe the data by means of an empirical correlation. Thus, with the restriction of describing the cooling vapor film temperature by the saturation temperature, the experimental data was fitted in a way similar to Yu and Yadigaroglu [14] by:

$$h = \begin{cases} h_0 e^{-a\zeta} & 0 < \zeta < 3 \\ h_0(e^{-a\zeta}+e^{-3a})/2 & 3 < \zeta < 5 \end{cases} \quad (13)$$

with

$$\zeta = (\Delta Z_{qf} - Z_{ref})/Z_{ref}. \quad (14)$$

Z_{ref} (chosen here at 5 cm) is an estimation for the distance downstream of the quench front at which the whole periphery of the wall dries out with rare wetted spots (cf. next section). At a smaller distance from the quench front the wall is often wetted and q''_w may reach the critical heat flux. That region was excluded from the present study. The values of h_0 and a based on the experiments are listed in Table 2 and plotted in Fig. 12.

The experimental values for h_0 given in Fig. 12 depend on the inlet velocity, and show a minor influence of the initial wall temperature. The experimental values for a shown in Fig. 12 are more dispersed. Still, dependency on V_{in} is shown.

LIQUID PENETRATION TO THE ANNULAR VAPOR FILM

Using the model described in Appendix B it became possible to estimate the quality and hence the vapor mass flux at the inlet to the annular film. Thus, with the use of the experimental data for the film thickness it became also possible to estimate the vapor velocity and try to derive the wall heat flux from known heat transfer

Table 2. The parameters of the heat transfer correlation, equation (13)

Test No.	Z (m)	h_0	a
1		220	0.22
2	1.045	380	0.36
3		480	0.28
4		400	0.41
5		470	0.41
6	1.045	500	0.38
7		520	0.38
8		410	0.38
9		460	0.36
10	1.045	520	0.38
11		560	0.31
12		210	0.46
13	1.07	240	0.44
14		320	0.36
15		390	0.33
16		320	0.32
17	1.07	350	0.28
18		370	0.31
19		430	0.24
20		340	0.25
21	1.07	390	0.20
22		360	0.29
23		400	0.29

correlations for laminar as well as turbulent single phase flow [15–17]. Unfortunately, we were left with the feeling that the actual heat flux is substantially augmented presumably due to liquid penetration into the inverted annular vapor film.

Attempts to detect the liquid penetration from the temperature trajectories raised doubts as to whether the signal sought can be effectively identified. A need for a direct evidence became apparent and the stainless-steel tube was replaced by a quartz tube that enabled the detection of liquid penetrations using direct optical means as described in ref. [10]. Unfortunately, doing so the common comparative base with the other results reported here is lost. Still, it is of interest to note the intensive liquid penetration into the vapor film as illustrated in Fig. 13. Here the probability, P, that more than 50% of a 0.5-mm laser beam transversing the tube adjacent to the inner wall is blocked by liquid, is given as a function of the distance from the quench front. The probability for the presence of liquid adjacent to the wall remains high, more than 80%, in the first 5 cm above the quench front confirming the choice of this range as the limit of frequent local wall wetting. Further downstream the probability of wetting the wall decreases almost exponentially. Still, clear evidence of liquid penetration with probability greater than 10% is shown up to 25 cm downstream from the quench front. Although we cannot identify the specific mechanism of liquid penetration from such data it is plausible to assume its responsibility for the wall heat flux augmentation in the region of $0 < \zeta < 5$.

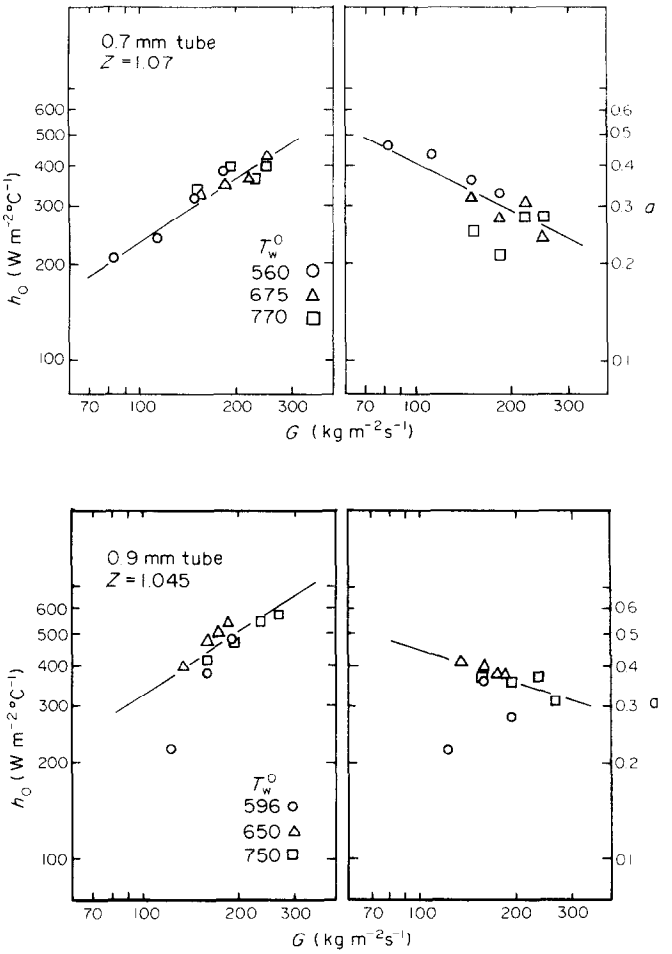

FIG. 12. The parameters of the heat transfer correlation.

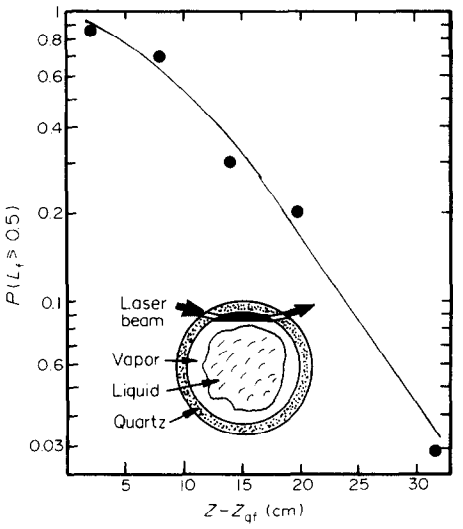

FIG. 13. The probability that more than 50% of a 0.5-mm laser beam is blocked by liquid in a quartz tube (I.D. = 12 mm, 1.5-mm wall, $G = 170$ kg m^{-2} s^{-1}, and $T = 600$°C).

REMARKS AND DISCUSSION

The present paper reports simultaneous measurements of the wall temperature and the vapor film thickness in the inverted annular film boiling regime, raising the confidence in identifying this special form of boiling regime. The raw data was elaborated to yield the wall heat flux, heat transfer coefficient, quench front velocity, quench front temperature and void fraction, and therefore may serve as a relatively complete comparative base for the development of theoretical models.

The bottom reflooding phase of a hypothetical accident in nuclear reactors, in which inverted annular boiling is expected, is characterized by residual heat sources that are almost constant during the quenching process. Thus, it is desired to compare computer codes programmed for safety studies with experimental data measured in channels with constant heat sources as is given here.

Judging the quality of the reported data it should be noted that apart from the experimental error it is

possible that the liquid core is helicoid and eccentric. Since the measurements were taken in a representative plane that includes the pipe's axis it is possible that our interpretations were misled by such an effect. Indeed, experience with a quartz tube showed helicity at relatively large distance from the quench front. Unfortunately, working with a stainless-steel tube, which is essential in the present test conditions, it is difficult to assess the phenomena.

It became apparent that further development of theoretical models should consider intensive turbulent processes at the liquid–vapor interface with liquid penetration into the vapor annulus associated with augmented heat transfer from the wall and additional evaporation rate within the vapor annulus. It also may be that the turbulence at the liquid–vapor interface augments the heat transfer into the liquid core referred to in the two-fluid model as the heat absorption potential. Clear understanding of the mechanism is still needed.

REFERENCES

1. W. L. Kirchner, Reflood heat transfer in light water reactors, Ph.D. thesis, Massachusetts Institute of Technology; NUREG-0106 (1976).
2. L. A. Arrieta and G. Yadigaroglu, UCFLOOD—Analytical model for bottom reflooding heat transfer in light water reactors, EPRI NP-756 (1978).
3. G. Yadigaroglu, K. P. Yu, L. A. Arrieta and R. Greif, Heat transfer during the reflooding phase of the LOCA—State of the art, EPRI 248–1 (1975).
4. E. Elias and G. Yadigaroglu, The reflooding phase of the LOCA in PWRs part II: rewetting and liquid entrainment, *Nucl. Safety* **19**, 160–175 (1978).
5. J. G. Collier, Heat transfer in the postburnout region and during quenching and reflooding, in *Handbook of Multiphase Systems* (edited by G. Hetsroni). Hemisphere, Washington (1982).
6. K. K. Fung, S. R. M. Gardiner and D. C. Groeneveld, Subcooled and low quality flow film boiling of water at atmospheric pressure, *Nucl. Engng Des.* **55**, 51–57 (1979).
7. M. Kawaji, Y. S. Ng and S. Banerjee, Flow regime and heat transfer measurements during reflooding with steady and oscillatory coolant injection, 2nd International Topical Meeting on Nuclear Reactor Thermohydraulics, Santa Barbara (1983).
8. R. S. Dougall and W. M. Rohsenow, Film boiling on the inside of vertical tubes with upward flow of the fluid at low qualities, MIT Report No. 9079-26 (1963).
9. E. Elias and P. L. Chambre, Inverted-annular film boiling heat transfer from vertical surfaces, *Nucl. Engng Design* **64**, 249–257 (1981).
10. Z. Edelman, D. Naot and E. Elias, Optical visualization of liquid penetration to the vapor film in inverted annular boiling, *Int. J. Heat Mass Transfer* **26**, 1715–1717 (1983).
11. Z. Edelman, Boiling heat transfer during bottom reflooding in PWR's, Ph.D. thesis, Technion—Israel Institute of Technology (1981).
12. K. P. Yu, An experimental investigation of the reflooding of a bare tubular test section, Ph.D. thesis, University of California, Berkeley (1978).
13. K. C. Chan and G. Yadigaroglu, Calculation of film boiling heat transfer above the quench front during reflooding, 19th National Heat Transfer Conference, Orlando, Florida (1980).
14. K. P. Yu and G. Yadigaroglu, Heat transfer immediately downstream of the quench front during reflooding, ASME paper 79-HT-48 (1979).
15. A. Quarmby and R. Quirk, Measurements of the radial and tangential eddy diffusivity of heat and mass turbulent flow in a plain tube, *Int. J. Heat Mass Transfer* **15**, 2309–2326 (1972).
16. N. Z. Azer, The ratio of eddy diffusivities for heat and momentum transfer for fully developed turbulent flow in concentric annuli, *Proc. of the* 1970 *Heat Transfer and Fluid Mechanics*, Institute of the Naval Postgraduate School, Monterey, California (1970).
17. D. Naot and W. Rodi, Numerical simulation of secondary currents in open channel flow with an algebraic stress turbulence model, SFB Report 80/T/187 (1981).
18. S. Banerjee and A. M. C. Chan, Separated flow models—I. Analysis of the average and local instantaneous formulations, *Int. J. Multiphase Flow* **6**, 1–24 (1980).
19. T. Saito, E. D. Hughes and M. W. Carbon, Multi-fluid modeling of annular two-phase flow, *Nucl. Engng Des.* **50**, 225–271 (1978).
20. G. B. Wallis, Annular two-phase flow—Part I: A simple theory, Part II: additional effects, *Am. Soc. Mech. Engrs, J. Basic Engng* **92** (1970).
21. R. A. Seban, R. Greif, D. Abdollahian and W. Peak, Comparison of experimental and predicted heat transfer for the data of UC-B reflood experiment, EPRI NP-1290 (1979).
22. D. Naot, Z. Edelman and E. Elias, Lower bound estimation for the vapor quality in local subcooled boiling, Center for Technological Education, Holon, Israel, Report CTED-844(N) (1984).

APPENDIX A: TWO-FLUID MODEL

A two-fluid model was constructed in order to examine the consistency between the experimental data for the wall heat flux and the film thickness. Thus, the six equations (i.e. the two sets of continuity, momentum and energy equations for the vapor annulus and the liquid cylindrical core) were solved subject to boundary and initial conditions that suit this specific purpose. The equations solved are [13, 18]:

$$\frac{\partial}{\partial Z}(\rho_g \alpha V_g) = \frac{\dot{m}_i}{\pi R^2} \tag{A1}$$

$$\frac{\partial}{\partial Z}[\rho_l(1-\alpha)V_l] = -\frac{\dot{m}_i}{\pi R^2} \tag{A2}$$

$$\frac{\partial}{\partial Z}(\rho_g \alpha V_g^2) + \frac{\partial p}{\partial Z} = -\alpha \rho_g g - \frac{\dot{m}_i}{\pi R^2} V_i - \frac{2}{R}(\tau_w + \sqrt{1-\alpha}\tau_i) \tag{A3}$$

$$\frac{\partial}{\partial Z}[\rho_l(1-\alpha)V_l^2] + (1-\alpha)\frac{\partial p}{\partial Z} = -(1-\alpha)\rho_l g - \frac{\dot{m}_i}{\pi R^2} V_i + \frac{2}{R}\sqrt{1-\alpha}\tau_i \tag{A4}$$

$$\frac{\partial}{\partial Z}(\rho_g \alpha V_g h_g) = \frac{\dot{m}_i}{\pi R^2} h_i + \frac{2}{R}(q''_{wg} - q''_{gl}\sqrt{1-\alpha}) \tag{A5}$$

and

$$\frac{\partial}{\partial Z}[\rho_l(1-\alpha)V_l h_l] = -\frac{\dot{m}_i}{\pi R^2} h_i + \frac{2}{R}(q''_{wl} + q''_{gl}\sqrt{1-\alpha}). \tag{A6}$$

Here the evaporation rate $\dot{m}_i$ is calculated from a heat balance applied to a thin layer adjacent to the water–vapor interface, expressing the fact that the radial heat conduction to the interior of the liquid core is restricted by a heat absorption potential q''_p

$$\frac{\dot{m}_i}{\pi R^2} = \max \begin{cases} \dfrac{2}{h_{fg} R}[q''_{wl} + \sqrt{1-\alpha}q''_{gl} - q''_p\sqrt{1-\alpha}] \\ 0 \end{cases} \tag{A7}$$

with q''_p estimated by $k_l(T_s - T_l)/(\sqrt{1-\alpha}R)$. Once the heat flux to the liquid surface becomes greater than the heat absorption potential $\dot{m}_i$ is no longer zero. The liquid interface reaches saturation temperature T_s, the vapor enthalpy just as it leaves the surface h_i becomes $h_{g,s}$ and equation (A6) turns by virtue of equation (A7) to

$$\frac{\partial}{\partial Z}[\rho_l(1-\alpha)V_l h_l] = -\frac{\dot{m}_i}{\pi R^2}h_{l,s} + \frac{2}{R}\sqrt{1-\alpha}\,q''_p \quad \text{(A8)}$$

as is expected. The vapor is assumed to leave the surface with the velocity V_i that equals the liquid velocity V_l.

The wall shear stress was calculated with Blasius' friction factor, and the shear stress at the interface was calculated with an estimation for the friction factor based on Saito [19] and Wallis [20]. The wall heat flux is split into two contributions. One is transferred by radiation directly to the liquid core:

$$q''_w = \frac{(T_w^4 - T_s^4)\sqrt{1-\alpha}}{\dfrac{1}{\varepsilon_l} + \left(\dfrac{1}{\varepsilon_w} - 1\right)\sqrt{1-\alpha}} \quad \text{(A9)}$$

with $\varepsilon_l = 0.96$ and $\varepsilon_w = 0.6$, and the other q''_{wg} is transferred to the gas and is given by equation (13) expressing the experimental data. Finally, to calculate the heat transferred from the gas to the liquid q''_{gl} we assume that the heat transfer augmentation referred to in the paper applies also to the interface and assumes equality between the heat transfer coefficients:

$$q''_{gl} = q''_{wg}\frac{T_g - T_s}{T_w - T_g} \quad \text{(A10)}$$

leaning again on the experimental data.

The initial conditions were derived from the experimental data using the estimation of the vapor quality downstream and quench front, X^+, as described in Appendix B.

APPENDIX B: QUENCH FRONT MODEL

To specify the liquid and vapor conditions at the inlet to the inverted annular regime we perform a heat balance. Assuming that the flow behind the quench front is steady it is possible to derive the equilibrium quality at the inlet to the quench front region X_e^- from a steady-state heat balance [21]:

$$X_e^- = \frac{1}{h_{fg}}\left[\frac{1}{\dot{m}}\int_0^{Z_{qf}} q'(Z)\,dZ - c_{pl}(T_s - T_{l,in})\right]. \quad \text{(B1)}$$

Then, a quasi-steady-state heat balance is performed for a control volume that contains the quench front and moves at the quench front velocity. The step in the equilibrium quality is obtained:

$$\Delta X_{qf} = \rho_w c_{pw} A_w V_{qf}(T_q - T_{rw})/(\dot{m}_r h_{fg}). \quad \text{(B2)}$$

Here a reduced mass flux is used:

$$\dot{m}_r = \dot{m}(V_{in} - V_{qf})/V_{in} \quad \text{(B3)}$$

and T_{rw} is the wetted wall temperature assumed to equal the saturation temperature. The equilibrium quality at the inlet to the inverted annular regime is then calculated:

$$X_e^+ = X_e^- + \Delta X_{qf}. \quad \text{(B4)}$$

To complete the specification we need an estimation for the vapor quality at the inlet to the inverted annular regime X^+. Two extreme values are available [22]:

$$0 < X^+ < \Delta X_{qf} \quad \text{(B5)}$$

where the upper bound represents a situation in which the vapor formed at the wall does not have enough time to transfer heat to the liquid phase, and the lower bound represents the situation where the vapor bubbles collapse transferring all the heat to the liquid phase. Estimation based on subcooled boiling correlations [22] suggests that X^+ is close to the upper bound. In the present work an estimate for X^+ was used as [22]:

$$X^+ = 0.75\Delta X_{qf} \quad \text{(B6)}$$

EBULLITION, ANNULAIRE INVERSEE DANS UN TUBE D'ACIER INOXYDABLE, AVEC DES SOURCES DE CHALEUR PERMANENTES

Résumé—On décrit des mesures simultanées de températures pariétales et d'épaisseurs de film de vapeur dans une ébullition en film annulaire inversée. Les données correspondent au 'reflooding' inférieur d'un tube unique uniformément chauffé par une source de chaleur électrique et permanente. Les essais sont conduits pour fournir le flux thermique à la paroi, le coefficient de transfert thermique, la vitesse du front de trempe, la température du font de trempe et la fraction de vide, grandeurs qui peuvent servir à une base relative complète pour le développement de modèles théoriques.

FILMSIEDEN BEI INVERSER RINGSTRÖMUNG IN EINEM ROHR AUS ROSTFREIEM STAHL MIT STATIONÄREN WÄRMEQUELLEN

Zusammenfassung—Es wird über die gleichzeitige Messung der Wandtemperaturen und der Dampffilmdicke beim Filmsieden in einer inversen Ringströmung berichtet. Die Daten stimmen mit denen überein, die sich beim Fluten eines Einzelrohres ergeben, welches mit einer stationären elektrischen Heizquelle gleichförmig beheizt wird. Die Rohdaten werden weiter verarbeitet, um die Wärmestromdichte an der Wand, den Wärmeübergangskoeffizienten, die Geschwindigkeit und die Temperatur der Quench-Front sowie den Dampfvolumenanteil zu berechnen, was als relativ vollständige Vergleichsgrundlage für die Entwicklung von theoretischen Modellen dient.

КОЛЬЦЕВОЕ КИПЕНИЕ ЖИДКОСТИ НА ПОВЕРХНОСТИ ТРУБЫ ИЗ НЕРЖАВЕЮЩЕЙ СТАЛИ, ОБОГРЕВАЕМОЙ ПОСТОЯННЫМ ТЕПЛОВЫМ ПОТОКОМ

Аннотация—Представлены данные по одновременному измерению температуры стенки и толщины пленки пара при кольцевом пленочном кипении жидкости на поверхности трубы. Данные соответствуют процессу кипения при повторном заливе поверхности одиночной трубы, обогреваемой источником постоянного электрического тока. В результате обработки экспериментальных данных определен тепловой поток на стенке, коэффициент теплоотдачи, скорость движения поверхности раздела жидкость-пар, температура на поверхности раздела и объемная доля паровой фазы, что может служить относительно достаточной базой для создания теоретической модели процесса.